EARTHQUAKE MAGNITUDE MEASUREMENTS FOR PUERTO RICO

UGGS AWARD NO. 02HQGR0054

June 2003

Dariush Motazedian and Gail Atkinson

Dept. Earth Sciences

Carleton University

1125 Colonel By Dr.

Ottawa, Ontario

CANADA K1S 5B6

613-520-2600 X1399

613-520-2569 (fax)

gma@ccs.carleton.ca

Earthquake magnitude measurements for Puerto Rico

Dariush Motazedian and Gail Atkinson

June, 2003

Introduction

In Puerto Rico, there has been a long-standing problem with regional magnitude determinations. What is really needed for hazard analysis is a moment-magnitude-based catalogue. The reported magnitudes for Puerto Rico earthquakes are mostly Md (magnitude based on duration calculated by PRSN) and mb (body wave magnitude). The seismic event catalogue for Puerto Rico is dominated by earthquakes with magnitude smaller than 5, for which conventional estimates of moment magnitude (such as the Harvard Centroid Moment Tensor solutions) are not available.

The Puerto Rico Seismic Network (PRSN), consisting of 13 vertical component short-period 1Hz natural frequency seismometers was installed in 1974. Digital time series have been recorded by the PRSN since 1991 in IASPEI format (16-bit A to D converter, 100 samples/Sec). More than 2000 time series recorded by the PRSN, from more than 300 events with M≥3.0 have been compiled. There is a strong motion network in Puerto Rico (PRSMN), which has been installed gradually since 1994, and now comprises 32 strong motion stations. The number of recorded acceleration time series is limited, since the earthquake ground motion must be strong enough to trigger these accelerographs. There has been a single **IRIS/USGS** station (SJG) operating in Puerto Rico since 1993; it includes five broadband seismometers (three-component), and one short period seismometer (three-component). The sampling rate of the short period three-component seismometers is 80 samples/sec. The highest sampling rate for the broadband seismometer data is 20 samples/sec (The sampling rate of the other broadband seismometers at station SJG is too low to be used for our study.). The purpose of this study is to use these available post-1991 digital data sources to develop a useful magnitude scale to apply to regional earthquake data for Puerto Rico.

Ideally, the magnitude scale should be closely correlated with moment magnitude. Based on the Brune (1970, 1971) point source model, the acceleration spectrum for an earthquake at a distance R is modeled as a point source with an ω^2 shape. The observed acceleration spectrum of shear waves of the earthquake, A(f), is (Aki, 1967; Brune, 1970; Boore 1983) :

$$A(f)=C\,M_0\,[(2\pi f)^2/[1+(f/f_0)^2]]\,[\exp(-\pi f\kappa)\exp(\pi f R/Q\beta)/R]\,S(f) \qquad (1)$$

where M_0, f_0 and R are seismic moment, corner frequency and distance (hypocentral) from the observation point, respectively. S(f) represents site amplification (=1 for a very hard rock site). The constant $C=\Re^{\theta\varphi} F V /(4\pi\rho\beta^3)$, where $\Re^{\theta\varphi}$ = radiation pattern (average value of 0.55 for shear waves), F= free surface amplification (2.0), V= partition onto two horizontal components (0.71), ρ= density and β is shear wave velocity (Boore, 1983). The term $\exp(-\pi f\kappa)$ is a high cut filter to model near-surface "*kappa*" effects: this is the commonly-observed rapid spectral decay at high frequencies. The quality factor, $Q(f)=[\log(e)\pi f]/(c\beta)$, is inversely proportional to anelastic attenuation, $c(f)$. The implied 1/R attenuation term is applicable for body-wave

spreading in a whole space and can be modified based on the geometric spreading behavior of seismic waves. The corner frequency, f_0, is given by

$$f_0=4.9e+6\,\beta\,(\Delta\sigma/M_0)^{1/3} \qquad (2)$$

where $\Delta\sigma$ is stress drop in bars, M_0 is in dyne-cm and β is shear wave velocity in km/s (Boore, 1983).

If we calculate the Fourier spectrum of a recorded time series, divide out frequency-dependent site amplification ($S(f)$), then play back the attenuation effects (including anelastic and geometric behaviors), all according to Equation 1, then we can obtain an estimate of the source spectrum, $A_0(f)$:

$$A_0(f) = A(f) / [[\exp(-\pi f\kappa)\exp(\pi f R/Q\beta)/R]\,S(f)] \qquad (3)$$

Where the acceleration source spectrum is:

$$A_0(f)=C\,M_0\,(2\pi f)^2/[1+(f/f_0)^2] \qquad (4)$$

Based on the Brune point source model (Equation 4) the displacement spectrum can be obtained by:

$$D_0(f) = (2\pi f)^{-2} A_0(f)$$

or

$$D_0(f)= CM_0/[1+f/f_0)^2] \qquad (5)$$

At low frequencies ($f << f_o$), the displacement spectrum would be:

$$D_0(f) = C\,M_0 \qquad (6)$$

Thus if we use the recorded data and Equation 3 to play back the attenuation effects (including anelastic and trilinear hinged geometric behaviors), then by using Equation 6, $\mathbf{M_0}$ and hence moment magnitude **M** can be calculated (where $\mathbf{M} = (\log_{10}M_0 - 16.05)/1.5$ (Hanks and Kanamori, 1979)). This approach to calculating moment magnitude can be employed for broadband records, from which low-frequency amplitudes ($f << f_o$) can be recovered. (Recorded time series on short-period seismometers do not have sufficient bandwidth for this approach.). We apply the recorded time series at the broadband SJG station for the calculation of seismic moment using Equation 6; this will produce single-station moment magnitude estimates that can be used to calibrate magnitude scales.

Moment Magnitude based on the displacement spectrum at lower frequencies

The vertical component of ground motion in the shear window is relatively unaffected by near-source amplifications (in comparison to the horizontal components) and thus we assume $S(f)=1$ for all vertical-component records. Using Equation 3, we played back the geometric spreading and anelastic behavior of Puerto Rico region for all of the vertical components recorded at the SJG broadband station. The input parameters are the regional attenuation parameters determined by empirical analysis of seismographic data for Puerto Rico (Motazedian, 2002; Motazedian and Atkinson, 2003), summarized as follows.

Geometric spreading. The Fourier amplitudes of Puerto Rico earthquakes follow a trilinear curve for attenuation, which has hinges at 75 and 100km (Motazedian and Atkinson 2003). The slope of the geometric attenuation is –1.0, 0.0 and –0.5 for R<75 km, 100≥R≥75 km and R>100 km, respectively.

Q values. The anelastic attenuation associated with this model is expressed by the regional quality factor $Q=359\,f^{0.59}$ (Motazedian and Atkinson 2003).

Other parameters. Shear wave velocity and density are assumed to be 3.6 km/sec and 2.8 g/cm^3 respectively.

In order to apply Equation 6 for the calculation of seismic moment, we obtain the constant D_0 for the flat portion of the displacement spectrum ($f \ll f_o$). The displacement spectrum at the very lowest frequencies, for which the calculated spectrum is not reliable, and at high frequencies, above the corner frequency, is not used in the calculation of D_0. Figure 1 shows the displacement spectrum of a **M**4.8 earthquake and the Brune source displacement spectrum model for that earthquake as an example; it can be seen that the flat portion of the spectrum covers the frequency band from about 0.1 to 0.8 Hz. To obtain the spectral amplitudes from which to determine the average D_0, a Butterworth filter with the order of 8 was applied to the source spectra to cut amplitudes above the high-cut limit of $f_h = f_0/3$, where a rough estimate of the corner frequency is made using Equation 2 with an assumed stress drop of 150 bars. A matching low-cut filter was used to cut frequencies < $f_h/5$. For example the Butterworth filter for **M**4.8, with the assumed corner frequency of 1.76, retains the spectral amplitudes for frequencies from 0.12 Hz to 0.59 Hz. Due to inter-event stress drop variability, the observed corner frequency may not always coincide with the estimated corner frequency used in the Butterworth filter. This is not critical, however, since the corner frequency estimate is used only to determine the frequency range over which the long-period spectral level can be confidently defined. The conservative use of $f_0/3$ to define the high-cut filter frequency means that a factor of three variability in actual corner frequency, corresponding to a factor of 27 in variability of stress drop (stress drop as low as 5 bars; see Equation 2), can be accommodated without biasing the moment estimate. For each record, the time series were processed as follows:

- Define S-window and pre-event noise (minimum 10 second noise window were used for calculation of signal to noise ratio). The S-window includes the strongest shaking and its coda.
- Remove any glitches.
- Taper the windowed time series using a 5% taper on each end of signal.
- Zero-Pad the time series to the next greatest power of 2.
- Transfer to frequency domain by application of Fast Fourier transform.
- Calculate instrument response based on the poles, zeros and constant for that specified component of the seismographic station.
- Remove the instrument response in the frequency domain by dividing the recorded spectrum by the instrument transfer function.
- Convert Fourier spectrum of velocity to Fourier spectrum of displacement (done in the same step as removal of instrument response).

- Discard data points at the frequencies showing signal to noise ratio less than 2. (Note: the noise window is normalized to the same length as the signal window to check the signal/noise ratio.)
- Smooth the Fourier spectrum by using a weighted 9-point smoothing algorithm.
- For a trial value of moment magnitude, apply a band pass filter (a Butterworth filter with the order of 8) to the displacement spectral amplitudes, based on the assumed corner frequency .
- Iteration of Equation 5 over seismic moment (for **M**=1 to **M**=8, in 0.1 unit increments) to determine the best-fit value of M_0. The iteration procedure finds the value of M_0 for which the area under the filtered displacement spectrum, according to the Brune model (Eqn. 5), most closely matches the area under the filtered observed displacement spectrum.
- Determine $\mathbf{M} = (\log 10\ M_0 - 16.05)/1.5$

It may be noted that the above procedure differs slightly from that used by Motazedian and Atkinson (2003) to calculate **M,** in that our current approach uses the Butterworth filter procedure described above to isolate the portion of the spectrum to use in calculating the moment, while Motazedian and Atkinson (2003) calculated moment from a few selected low-frequency points.

Figure 2 shows **M** versus catalogue magnitude, where **M** is calculated based on the recorded waveforms at SJG. Because the moment magnitudes are calculated from a single station, they have significant uncertainty. The reported catalogue magnitude for virtually all (>99%) of the earthquakes with magnitude <4.0 is Md (duration magnitude), while the reported catalogue magnitude for all of the earthquakes with magnitude ≥4.0 is mb. There is a systematic difference between **M** and catalogue magnitude (M_{cat}), with the catalogue magnitude exceeding moment magnitude by about 0.4 units on average.

To verify the attenuation model used in our calculations of moment magnitude, we plot the residuals ($\mathbf{M} - M_{cat} + 0.4$) versus depth and distance in Figures 3 and 4. (Note: we correct for the overall average difference of 0.4 in magnitudes since it is the trend with distance that we wish to investigate). As Figures 3 and 4 show there are no obvious distance-dependent or depth-dependent trends in the obtained residuals, indicating that the attenuation corrections used in our moment magnitude calculations are working well.

Table 1 lists the calculated **M** and the reported catalogue magnitudes for events in Puerto Rico (M_l ,discussed later, is also given). There are a few of the larger events in our catalogue for which an independent estimate of moment magnitude is available. Table 2 presents the comparison between our calculated **M** and these more reliable global estimates based on CMT solutions. The largest catalogue event has a moment magnitude (CMT) of 6.0, while our estimated **M** for that earthquake is 5.9. Overall, Table 2 indicates that our estimated **M** values are reasonably close to CMT moment magnitude, especially considering that our estimates are based on a single station. An exception is the large difference between our estimate of **M** (4.6) and the CMT value (5.2) for the earthquake on 1998/08/10; the large distance (500 km) from SJG may have been a factor in this discrepancy.

An Intermediate-period Magnitude, M_I

The difficulty with the calculation of moment magnitude based on the displacement spectrum at lower frequencies is that short-period network data, such as those of the PRSN (with a large number of recorded waveforms), do not generally extend to sufficiently low frequencies to satisfy the $f<<fo$ constraint. To get around this difficulty, Chen and Atkinson (2002) proposed an alternative magnitude measure, M_I, which would track **M**. Consider Equation 4 at f = 1Hz:

$$A_0(1)=CM_0 4\pi^2/[1+(1/f_0)^2] \quad (7)$$

If we assume a constant value of 150 bars for $\Delta\sigma$, and use Equation 2 to relate $\Delta\sigma$ to f_0, then Equation 7 can be solved numerically by trial and error to find an estimate of M_0, which we will denote here as $M_0(1)$ (to indicate that it is an estimate only, obtained at a frequency of 1 Hz). The estimate $M_0(1)$ will only equal the actual M_0 for events with spectra that follow the assumed underlying Brune model spectra with $\Delta\sigma$=150 bars; however, the value of $M_0(1)$ obtained is not sensitive to stress drop for small events (as will be discussed later.). The estimated moment magnitude can then be calculated using M_I= (2/3) log $M_0(1)$- 10.7, where the notation M_I is used to indicate that this magnitude definition is based on the estimate $M_0(1)$ (Chen and Atkinson, 2002). M_I is an intermediate-period magnitude scale that will equal moment magnitude for earthquakes following the Brune model (Chen and Atkinson, 2002, page888, Figure 2). Because the source spectrum amplitudes at frequencies lower than the corner frequency are independent of stress drop (recall $A(f)_{f<<f_0}=CM_0 4\pi^2 f^2$), the calculated M_I is not sensitive to stress drop for small events (**M**<5), for which $f_0 > 1$.

Chen and Atkinson (2002) applied this approach to a large number of worldwide earthquakes (more than 3000 earthquakes). In order to evaluate the applicability of their conclusion that M_I=**M** for small to moderate earthquakes, specifically for Puerto Rico, we used stochastic finite fault modeling (Appendix A) to simulate a large number of earthquakes and investigate the validity of M_I=**M** for Puerto Rico. Acceleration time series for earthquakes with magnitudes from **M**2.0 to **M**8.0 and hypocentral distances from 10 km to 500 km were simulated as described by Motazedian and Atkinson (2003). Simulations were performed in magnitude steps of 0.5 units. For each simulated earthquake fault plane, we performed simulations for 7 azimuthal profiles, using 15 different distances of the observation point for each profile, as shown in Figure 5. The input parameters are the regional attenuation parameters for Puerto Rico (Motazedian, 2002; Motazedian and Atkinson, 2003). The following describes the input parameters to the calculation of M_I for the simulated Puerto Rico earthquakes.

Stress parameter. As discussed above the stress drop does not affect calculation of M_I for small to moderate earthquakes (**M**<5). We consider the general stress drop $\Delta\sigma$ =150 bars as defined by Chen and Atkinson (2002).

Kappa. High frequency amplitudes are reduced through the kappa operator (Anderson and Hough 1984) by applying the factor $\exp(-\pi f\kappa)$. This factor, which models near surface attenuation, generally varies between 0.02 and 0.04 for soft rock sites (Anderson and Hough; 1984, Boore et al, 1992; Atkinson and Silva, 1997; Boore and Joyner, 1997). $\exp(-\pi f\kappa)$ is a high cut filter which does not affect calculation of spectrum at 1 Hz ($\exp(-\pi f\kappa)\approx 1$ for f=1 Hz). κ= 0.03 is adopted as a compromise between regional estimates.

Site amplification. The regional site amplification, $S(f)$, is assumed to be as given in Motazedian and Atkinson (2003). This represents regional crustal and near-surface amplification and is estimated from the H/V ratio. At 1 Hz, S=1.4 for horizontal components and S=1 for the vertical component.

Hypocenter. A random hypocenter location is assumed for the simulations. For each magnitude we simulated five events with a random location of hypocenter.

Other parameters. Shear wave velocity and density are assumed 3.6 km/sec and 2.8 g/cm^3 respectively. The fault dip has been considered 90°. The length and width of faults are calculated from the target moment magnitude based on the Wells and Coppersmith (1994) empirical formulas between magnitude and fault size. The sampling rate has been considered 100 samples/sec. A random slip distribution is assumed. The geometric spreading and anelastic attenuation are as described in the previous section for the calculation of **M**.

We simulated 650 vertical component acceleration time series for magnitudes from **M**2.0 to **M**8.0 and distances from 10 km to 500 km. M_I was obtained for all of the simulated acceleration time as described above. Figure 6 shows the obtained relationship between M_I and **M**. This figure shows that M_I is expected to be a good estimate of **M** for small to moderate earthquakes, up to **M**5.0. For larger magnitudes the deviation of M_I from **M** becomes large due to finite fault effects: for **M**>5 the Brune point source model is not generally applicable. The result of this time series simulation based on the Puerto Rico attenuation parameters confirms that we expect M_I=**M** for small to moderate earthquakes as proposed by Chen and Atkinson (2002).

Calculation of M_I for Puerto Rico earthquakes

Most of the recorded time series at seismographic stations in Puerto Rico are vertical component only. The vertical component of ground motion in the shear window is relatively unaffected by near-source amplifications and thus we assume S(1Hz)=1 for all vertical-component records. The vertical component short-period records were processed using the same steps as described above for the broadband records. After playing back the attenuation effects (Equation 3) to obtain the source spectrum of acceleration for each record, we determined M_I for each event as follows:

- Apply a band pass filter to the acceleration source spectra, centered at 1 Hz (a Butterworth filter with the order of 8 from 0.7Hz to 1.3 Hz)
- Iteration of Equation 7 over $M_0(1)$ (for M_I=1 to M_I=8, in 0.1 unit increments) to determine the best-fit value of $M_0(1)$. The iteration procedure finds the value of $M_0(1)$ for which the area under the filtered acceleration spectrum, according to the Brune model (Eqn. 4), most closely matches the area under the filtered observed acceleration spectrum.
- Average the calculated $M_0(1)$ over all of stations for each event.
- Determine $M_I = (\log_{10}M_0(1) - 16.05)/1.5$

Figure 7 shows the filtered acceleration source spectrum of a **M**4.8 earthquake after application of the above-mentioned procedures, in comparison to the Brune source acceleration spectrum model for that earthquake as an example. The total area under both curves is the same. Figure 8 shows M_l versus catalogue magnitude for earthquakes in Puerto Rico. There is a systematic difference between M_l and catalogue magnitude, with the average difference of 0.4 units. Figure 9 compares M_l with **M**. Figure 9 indicates that M_l =**M** for **M**≤5.0.

Conclusion

M, which is moment magnitude based on the displacement spectrum at lower frequencies, has been estimated from the recorded waveforms at a broadband station in Puerto Rico. Our estimates of moment magnitude agree reasonably well with independent global estimates for the few earthquakes that are large enough to have independent moment estimates. We also calculated M_l, which is based on the amplitude of acceleration source spectra at 1 Hz, and makes better use of the available short-period seismographic data in Puerto Rico. Both simulations and actual data show that **M** = M_l for small to moderate earthquakes (**M**≤5.0). The values of both **M** and M_l are, on average, 0.4 units smaller than reported catalogue magnitudes Md or mb. It is recommended that M_l be used as a regional magnitude scale for Puerto Rico earthquakes.

References

Aki, K. (1967). Scaling law of seismic spectrum, **J**. Geophys. Res. 72, 1217-1231.

Anderson, J. and S. Hough (1984). A model for the shape of the Fourier amplitude spectrum of acceleration at high frequencies. Bull. Seism. Soc. Am., **74**, 1969-1993.

Atkinson, G. and W. Silva (1997). Empirical source spectra for California earthquakes. Bull. Seism. Soc. Am., **87**, 97-113.

Boore, D. (1983). Stochastic simulation of high-frequency ground motions based on seismological models of the radiated spectra. Bull. Seism. Soc. Am., **73**, 1865-1894

Boore, D. and W. Joyner (1997). Site amplifications for generic rock sites. Bull. Seism. Soc. Am., **87**, 327-341.

Boore, D., W. Joyner and L. Wennerberg (1992). Fitting the stochastic omega-squared source model to observed response spectra in western North America: trade-offs between stress drop and kappa. Bull. Seism. Soc. Am., **82**, 1956-1963.

Brune, J. (1970). Tectonic stress and the spectra of seismic shear waves from earthquakes. J. Geophys. Res., **75**, 4997-5009.

Brune, J. (1971). Correction. J. Geophys. Res., 76, 5002.

Chen, S. and G. Atkinson (2002). Global Comparisons of Earthquakes Source Spectra. Bull. Seism. Soc. Am., **92**, 885-895.

Hanks, T. and H. Kanamori (1979). A moment magnitude scale. J. Geophys. Res., **84**, 2348-2350.

Motazedian, D. (2002). Development of ground motion relations for Puerto Rico using the stochastic finite-fault method. Ph.D. Thesis, Carleton University, Ottawa.

Motazedian, D. and G. Atkinson (2003). Ground motion relations for Puerto Rico, Geological Soc. Am. Special Issue on Neotectonic of Puerto Rico, in press.

Wells, D. and K. Coppersmith (1994). New empirical relationships among magnitude, rupture length, rupture width, rupture area, and surface displacement. Bull. Seism. Soc. Am., **84**, 974-1002.

Table 1. List of earthquakes in Puerto Rico from 1993 through 2002 with the reported moment magnitude in catalogue, estimated **M** and M_1.

mb: Body wave Magnitude

Md: Duration Magnitude

ML: Local Magnitude

Mw: Moment magnitude from global CMT solution

M: Moment magnitude based on the displacement spectra

M_1: Magnitude based on 1 Hz frequency

Date			Location		Depth	Catalogue	Magnitude	M_1	M
Y	M	D	Lat.	Lon.	(km)	Magnitude	Type		
1993	1	1	19.63	-64.45	10	4.0	mb	3.9	**3.9**
1993	1	7	19.51	-64.40	10	4.6	mb	3.9	**3.9**
1993	1	16	19.37	-64.38	33	4.1	mb	3.8	**3.9**
1993	4	13	18.95	-70.69	79	4.7	mb	4.7	**4.3**
1993	5	27	19.11	-63.31	39	4.6	Ms	4.0	**4.1**
1993	7	22	18.58	-69.00	109	4.8	mb	4.6	**4.6**
1993	8	10	19.35	-64.89	36	4.5	mb	4.2	**4.4**
1993	9	30	18.75	-62.80	33	4.3	mb	3.3	**3.6**
1993	10	3	17.80	-62.75	10	4.2	Md	3.6	**3.8**
1993	10	18	18.66	-64.45	30	4.3	mb	4.1	**4.0**
1993	10	24	19.68	-70.38	33	4.0	mb	4.2	**4.1**
1993	11	5	19.02	-66.01	48	4.9	mb	4.5	**4.6**
1993	11	8	19.20	-68.08	10	4.6	mb	4.1	**4.1**
1994	1	6	18.05	-68.37	87	4.0	mb	4.1	**4.2**
1994	1	8	18.22	-64.33	103	4.8	mb	3.9	**3.8**
1994	1	13	18.84	-66.18	47	4.0	mb	3.7	**3.8**
1994	1	18	18.58	-68.82	163	4.6	mb	4.3	**4.3**
1994	1	21	19.67	-64.43	10	4.0	mb	3.7	**3.7**
1994	2	25	19.25	-64.23	33	4.3	mb	3.5	**3.8**
1994	2	25	19.25	-64.33	32	4.9	mb	4.2	**4.1**
1994	3	1	19.39	-65.16	10	4.3	mb	3.7	**3.9**
1994	3	10	17.81	-65.35	10	4.1	mb	3.8	**3.9**
1994	4	21	18.00	-62.88	75	5.0	mb	4.7	**4.8**
1994	5	1	17.93	-64.70	162	4.3	mb	3.8	**3.9**
1994	6	25	19.01	-66.83	46	4.7	mb	4.3	**4.4**
1994	6	25	18.94	-66.68	33	4.0	Md	3.3	**3.4**
1994	7	11	19.23	-66.76	10	4.4	mb	3.9	**4.0**
1994	7	17	17.63	-62.94	131	4.2	mb	3.8	**4.0**
1994	9	23	18.43	-61.53	31	4.4	Md	3.9	**4.1**
1994	10	12	18.24	-68.37	107	4.4	mb	4.1	**4.1**
1994	11	17	17.92	-68.69	33	4.5	mb	4.0	**4.1**
1994	11	17	18.62	-68.34	81	4.7	mb	4.6	**4.4**
1994	11	30	19.53	-64.60	19	4.5	mb	4.2	**4.3**
1995	1	1	19.22	-69.42	42	4.8	mb	4.7	**4.7**

1995	1	18	18.89	-70.33	91	5.0	mb	4.7	**4.9**
1995	2	1	18.19	-68.36	179	4.6	mb	4.1	**4.1**
1995	2	16	18.88	-64.18	33	4.1	mb	3.8	**3.8**
1995	2	16	19.48	-65.79	33	4.0	mb	3.7	**3.8**
1995	5	4	18.89	-64.29	47	4.5	Md	3.8	**3.9**
1995	6	20	17.88	-62.85	100	4.2	mb	4.0	**4.1**
1995	7	9	19.62	-67.14	33	4.6	mb	3.8	**4.0**
1995	7	26	19.19	-64.67	52	4.6	mb	4.3	**4.3**
1995	7	28	19.57	-69.62	33	4.2	mb	4.0	**4.0**
1995	8	13	19.41	-69.36	10	4.4	mb	4.1	**4.1**
1995	9	19	18.79	-62.53	10	4.7	mb	3.8	**4.1**
1995	10	8	19.01	-66.96	46	4.8	Md	4.3	**4.6**
1995	10	31	19.70	-69.75	62	4.8	mb	4.2	**4.0**
1995	12	9	18.89	-65.71	50	4.2	mb	3.9	**3.9**
1995	12	31	18.44	-64.60	33	4.7	ML	4.1	**4.2**
1996	1	2	18.79	-62.70	33	4.5	ML	3.6	**3.9**
1996	1	24	18.19	-69.99	50	4.4	mb	3.9	**3.8**
1996	3	20	19.22	-66.75	33	4.1	mb	3.9	**3.9**
1996	4	9	18.88	-69.72	88	4.1	mb	4.1	**4.0**
1996	4	24	18.88	-70.32	82	5.2	mb	4.6	**4.6**
1996	5	11	19.31	-64.96	35	5.1	Mw	4.8	**5.2**
1996	5	12	18.48	-63.84	33	4.7	mb	4.4	**4.4**
1996	5	14	18.94	-65.08	33	4.2	mb	4.1	**4.1**
1996	5	29	18.06	-69.64	52	4.0	mb	4.1	**4.1**
1996	6	11	17.25	-68.28	33	5.5	mb	4.6	**4.9**
1996	6	12	20.03	-70.19	33	4.5	mb	4.3	**4.1**
1996	7	21	18.30	-62.41	60	4.5	mb	4.2	**4.1**
1996	10	17	19.02	-69.11	33	4.4	mb	4.2	**4.1**
1996	11	1	18.60	-64.28	33	4.4	mb	3.8	**3.7**
1996	11	6	18.85	-64.32	21	5.1	mb	4.6	**4.8**
1996	11	8	18.04	-68.53	73	4.8	mb	4.4	**4.4**
1996	12	4	19.04	-69.26	108	4.2	mb	4.2	**4.2**
1997	2	24	19.32	-69.23	90	4.5	mb	4.0	**3.9**
1997	3	17	18.91	-62.79	33	4.1	Md	4.4	**4.5**
1997	4	5	19.08	-63.12	33	4.3	mb	3.7	**4.0**
1997	5	14	19.63	-70.29	54	4.7	mb	4.6	**4.6**
1997	7	30	18.00	-70.32	10	4.9	mb	3.9	**4.2**
1997	10	12	18.58	-66.22	100	3.7	Md	3.3	**3.3**
1997	10	15	18.67	-67.44	10	3.3	Md	3.1	**3.1**
1997	10	24	17.99	-65.31	5	3.2	Md	2.9	**2.8**
1997	11	2	19.24	-66.34	33	4.3	mb	4.1	**4.2**
1997	11	21	18.56	-67.01	100	3.7	Md	3.1	**3.1**
1997	12	6	18.75	-67.34	80	3.5	Md	3.1	**3.1**
1997	12	21	18.58	-66.54	80	3.1	Md	2.9	**2.7**
1997	12	26	18.18	-68.44	94	4.7	mb	4.2	**4.1**
1997	12	27	17.82	-66.10	5	3.0	Md	2.8	**3.0**
1997	12	31	17.84	-66.10	10	3.0	Md	2.7	**2.9**
1997	12	31	18.50	-66.13	100	3.1	Md	2.8	**2.8**

1998	1	16	18.55	-66.12	106	3.1	Md	2.9	**2.7**
1998	1	17	18.96	-64.61	72	3.5	Md	3.1	**3.1**
1998	1	18	19.17	-64.66	25	4.4	mb	4.2	**4.0**
1998	1	18	18.98	-64.64	52	3.6	Md	3.1	**3.1**
1998	1	19	18.20	-67.17	13	3.7	Md	3.2	**3.2**
1998	1	20	19.03	-65.09	97	3.5	Md	3.1	**3.2**
1998	2	13	19.09	-66.09	27	3.0	Md	2.9	**2.8**
1998	2	13	18.05	-65.46	14	3.7	Md	3.4	**3.4**
1998	2	18	18.37	-64.97	24	3.3	Md	3.0	**2.9**
1998	2	19	19.15	-66.43	37	3.0	Md	2.9	**2.7**
1998	3	10	18.04	-65.60	1	3.2	Md	2.9	**2.7**
1998	3	12	18.14	-66.70	60	3.5	Md	3.1	**3.1**
1998	3	19	18.86	-66.02	56	3.1	Md	2.9	**2.7**
1998	3	25	19.38	-67.09	25	4.9	mb	4.3	**4.5**
1998	3	27	18.66	-64.25	50	3.4	Md	3.1	**3.1**
1998	4	1	18.15	-67.34	0	3.0	Md	2.9	**2.7**
1998	4	10	18.15	-66.85	16	3.0	Md	2.8	**2.7**
1998	4	15	18.18	-64.20	25	3.5	Md	3.0	**3.0**
1998	4	15	17.92	-65.54	2	3.8	Md	3.6	**3.6**
1998	4	16	17.78	-65.61	2	3.1	Md	3.0	**3.0**
1998	4	16	18.02	-65.63	0	3.6	Md	3.0	**3.0**
1998	4	16	18.07	-65.54	0	3.0	Md	2.8	**2.6**
1998	4	17	19.08	-67.36	22	3.1	Md	3.0	**2.8**
1998	4	18	18.65	-67.49	1	3.6	Md	3.2	**3.2**
1998	4	20	18.67	-66.72	79	3.4	Md	2.9	**2.9**
1998	4	25	19.00	-67.49	25	3.3	Md	3.0	**2.9**
1998	4	26	18.22	-67.09	20	3.6	Md	3.0	**3.1**
1998	4	26	19.07	-66.41	30	3.3	Md	2.9	**2.9**
1998	4	29	18.16	-65.87	87	3.8	Md	3.5	**3.5**
1998	4	30	18.71	-65.04	71	3.2	Md	3.0	**2.8**
1998	5	12	18.04	-65.55	0	3.1	Md	2.8	**2.7**
1998	5	14	17.95	-64.67	25	3.6	Md	3.0	**3.1**
1998	5	15	19.14	-66.49	49	3.5	Md	3.2	**3.2**
1998	5	22	19.22	-66.70	36	3.8	Md	3.3	**3.3**
1998	5	24	19.11	-67.17	25	3.6	Md	2.9	**3.0**
1998	5	27	19.23	-66.65	24	3.7	Md	3.3	**3.4**
1998	5	29	19.66	-66.95	10	3.6	Md	3.3	**3.4**
1998	6	13	17.75	-64.14	30	3.6	Md	3.2	**3.2**
1998	6	13	19.48	-66.36	48	3.9	Md	3.3	**3.3**
1998	6	14	18.62	-65.27	48	3.9	Md	3.5	**3.5**
1998	6	18	18.08	-65.53	0	3.3	Md	2.9	**2.8**
1998	6	21	18.97	-64.30	58	3.6	Md	3.1	**3.2**
1998	6	23	19.42	-65.28	49	3.8	Md	3.4	**3.5**
1998	6	24	17.74	-66.33	17	3.6	Md	3.0	**3.1**
1998	6	25	18.68	-65.99	68	3.1	Md	2.9	**2.7**
1998	7	4	18.32	-65.95	135	3.3	Md	2.9	**2.8**
1998	7	5	18.85	-67.23	18	3.0	Md	2.9	**2.7**
1998	7	19	18.30	-65.10	131	4.6	mb	3.6	**3.8**

1998	7	25	19.12	-66.11	15
1998	7	27	18.71	-66.51	25
1998	7	28	18.69	-65.00	25
1998	8	2	18.84	-67.27	13
1998	8	3	18.61	-67.44	12
1998	8	4	19.23	-64.66	60
1998	8	4	19.13	-64.51	56
1998	8	5	19.23	-64.66	60
1998	8	8	18.01	-66.61	13
1998	8	9	19.74	-70.00	33
1998	8	9	18.97	-64.93	22
1998	8	9	18.85	-64.55	95
1998	8	10	18.65	-70.54	58
1998	8	10	19.16	-64.77	72
1998	8	10	19.30	-64.74	25
1998	8	11	19.21	-66.14	25
1998	8	26	18.75	-65.99	69
1998	8	28	18.16	-68.26	82
1998	8	30	18.69	-70.27	33
1998	9	2	17.96	-66.34	9
1998	9	3	17.94	-66.33	8
1998	9	12	17.94	-66.32	6
1998	10	10	18.25	-66.29	6
1998	10	15	18.49	-70.47	68
1998	10	15	18.86	-65.16	53
1998	10	18	17.96	-65.68	5
1998	10	22	18.92	-65.14	59
1998	10	23	18.87	-64.38	33
1998	10	23	19.50	-64.55	65
1998	10	24	18.86	-64.32	56
1998	10	24	18.62	-66.73	19
1998	10	29	18.20	-65.94	14
1998	11	1	19.04	-65.23	45
1998	11	1	19.14	-65.13	67
1998	11	3	18.84	-65.07	25
1998	11	4	18.75	-65.93	73
1998	11	9	19.30	-65.25	75
1998	11	11	18.24	-67.04	17
1998	11	15	18.82	-66.25	35
1998	11	16	18.90	-67.38	58
1998	11	21	18.84	-65.23	72
1998	11	23	18.72	-66.12	25
1998	11	24	19.14	-67.78	33
1999	1	18	18.86	-67.22	33
1999	1	25	16.89	-62.50	140.3
1999	1	25	19.50	-66.69	50.1
1999	1	27	18.94	-63.26	33
1999	4	20	18.58	-65.37	91.8

3.1	Md
3.1	Md
3.1	Md
3.1	Md
3.3	Md
3.8	Md
3.6	Md
3.7	Md
3.0	Md
4.5	mb
3.5	Md
3.6	Md
5.2	Mw
3.7	Md
3.6	Md
3.0	Md
3.6	Md
4.5	mb
4.2	mb
3.3	Md
3.2	Md
3.2	Md
3.2	Md
4.4	mb
3.6	Md
3.2	Md
3.6	Md
4.0	Md
4.1	mb
4.6	mb
3.4	Md
3.0	Md
3.7	Md
3.6	Md
3.4	Md
3.1	Md
3.7	Md
3.9	Md
3.1	Md
3.1	Md
3.1	Md
3.1	Md
4.4	mb
5.0	Mw
4.6	mb
4.6	mb
4.1	mb
4.2	mb

3.0	**3.0**
2.9	**2.8**
3.0	**3.0**
3.0	**2.8**
3.0	**3.1**
3.7	**3.7**
3.2	**3.2**
3.5	**3.6**
2.9	**2.9**
3.8	**3.9**
3.1	**3.1**
3.3	**3.3**
4.5	**4.4**
3.5	**3.5**
3.2	**3.2**
2.9	**2.7**
3.2	**3.2**
3.9	**3.9**
3.8	**3.9**
2.7	**2.7**
2.6	**2.7**
2.7	**2.7**
2.6	**2.7**
4.4	**4.2**
3.1	**3.1**
2.7	**2.6**
3.2	**3.2**
3.6	**3.6**
3.9	**3.9**
4.1	**4.0**
2.8	**2.8**
2.5	**2.5**
3.2	**3.3**
3.3	**3.4**
2.9	**2.9**
2.8	**2.7**
3.3	**3.3**
3.4	**3.4**
2.8	**2.7**
3.0	**3.0**
2.9	**2.8**
2.8	**2.7**
4.0	**4.1**
4.6	**4.8**
3.7	**4.1**
3.9	**4.1**
4.0	**4.1**
3.5	**3.7**

1999	8	5	18.88	-67.18	71.6	4.3	mb	3.9	**4.0**
1999	8	7	18.76	-66.86	63.4	4.5	mb	4.1	**4.2**
1999	10	28	18.72	-67.25	33	4.1	mb	3.8	**3.9**
1999	12	20	17.31	-61.71	58.8	5.4	mb	5.0	**5.0**
2000	1	6	18.26	-68.32	178	4.0	Md	3.6	**3.7**
2000	1	9	17.94	-67.00	28	3.1	Md	2.9	**2.8**
2000	1	9	18.77	-67.25	68	3.2	Md	2.9	**2.9**
2000	1	13	18.97	-66.58	45	3.1	Md	2.9	**2.8**
2000	1	18	17.93	-65.66	4	3.1	Md	2.7	**2.7**
2000	1	18	18.93	-68.10	10	3.8	Md	3.2	**3.3**
2000	1	22	18.63	-66.88	12	3.0	Md	2.9	**2.6**
2000	1	25	19.61	-68.06	69	4.1	Md	3.7	**3.7**
2000	1	26	19.00	-67.76	34	3.0	Md	2.9	**3.0**
2000	1	29	18.89	-64.31	50	4.4	Md	4.1	**4.1**
2000	2	2	18.28	-66.23	74	3.0	Md	2.7	**2.6**
2000	2	4	19.48	-68.05	15	3.7	Md	3.1	**3.3**
2000	2	4	17.86	-67.04	28	3.2	Md	2.9	**2.9**
2000	2	6	17.99	-65.55	4	3.1	Md	2.8	**2.7**
2000	2	9	18.69	-67.52	2	3.5	Md	3.1	**3.2**
2000	2	10	18.07	-65.86	7	3.8	Md	3.4	**3.4**
2000	2	21	18.32	-67.88	108	4.4	mb	4.2	**4.0**
2000	2	26	18.93	-65.90	76	3.9	Md	3.0	**3.2**
2000	3	2	18.89	-65.18	42	3.7	Md	3.3	**3.3**
2000	3	5	18.91	-66.85	10	3.2	Md	2.8	**2.7**
2000	3	6	18.89	-66.40	46	3.0	Md	3.0	**2.7**
2000	3	6	18.13	-66.92	13	3.2	Md	3.0	**2.8**
2000	3	8	18.08	-67.11	18	3.0	Md	2.9	**2.7**
2000	3	8	19.16	-66.48	41	3.6	Md	2.9	**2.9**
2000	3	9	17.83	-65.66	8	3.4	Md	2.7	**2.8**
2000	3	14	18.01	-67.07	5	3.5	Md	2.9	**2.9**
2000	3	15	19.72	-66.04	72	3.9	Md	3.4	**3.5**
2000	3	20	18.41	-66.62	119	3.9	Md	3.5	**3.5**
2000	3	25	19.58	-68.15	25	3.8	Md	3.2	**3.2**
2000	3	25	19.26	-67.55	14	3.4	Md	3.1	**3.0**
2000	3	30	18.82	-68.01	46	4.3	Md	3.8	**3.8**
2000	4	4	18.97	-67.31	4	3.3	Md	3.0	**3.0**
2000	4	7	18.27	-67.58	6	3.3	Md	3.0	**2.9**
2000	4	8	18.16	-67.36	18	3.4	Md	2.9	**3.0**
2000	4	10	18.95	-64.23	84	4.0	Md	3.5	**3.6**
2000	4	10	18.67	-66.80	25	3.8	Md	2.9	**3.1**
2000	4	13	19.64	-63.29	33	4.2	mb	3.6	**3.8**
2000	4	18	19.08	-69.52	89	4.5	mb	3.8	**3.9**
2000	4	30	18.46	-67.97	22	3.6	Md	2.9	**3.0**
2000	5	3	17.67	-62.86	200	3.6	Md	3.3	**3.4**
2000	5	4	17.80	-65.62	3	3.3	Md	2.9	**2.9**
2000	5	8	19.45	-68.50	33	4.5	mb	3.7	**3.8**
2000	5	20	19.38	-67.26	56	3.8	Md	3.3	**3.4**
2000	5	26	19.04	-63.88	10	3.8	Md	3.4	**3.5**

2000	6	1	19.42	-65.42	49	4.6	Md	4.1	4.5
2000	6	18	17.93	-66.84	16	3.1	Md	2.9	2.8
2000	6	23	19.41	-65.19	76	3.6	Md	3.4	3.4
2000	6	24	18.08	-65.73	3	3.2	Md	2.7	2.7
2000	6	25	19.39	-65.11	66	3.8	Md	3.0	3.2
2000	7	5	18.40	-65.89	34	3.5	Md	2.8	2.9
2000	7	7	18.93	-66.76	53	3.3	Md	2.9	2.9
2000	7	24	18.15	-67.01	21	3.3	Md	2.8	2.9
2000	7	26	17.85	-61.51	33	4.0	mb	3.6	3.8
2000	7	28	18.70	-64.29	71	4.1	Md	3.6	3.6
2000	7	28	18.93	-64.68	62	4.4	mb	4.3	4.2
2000	7	29	17.84	-68.70	33	4.4	mb	4.3	4.3
2000	7	30	18.79	-69.42	87	3.9	mb	3.5	3.5
2000	7	31	18.77	-64.65	25	4.0	Md	3.2	3.3
2000	8	1	17.46	-68.24	117	4.2	Md	3.5	3.6
2000	8	2	18.39	-66.65	13	3.6	Md	2.8	2.9
2000	8	12	18.03	-66.60	15	3.6	Md	2.8	2.8
2000	8	15	19.16	-66.84	57	3.3	Md	3.0	3.0
2000	8	16	18.40	-65.91	105	3.2	Md	2.7	2.6
2000	8	17	18.11	-64.74	60	3.3	Md	2.7	2.7
2000	8	19	18.06	-65.51	0	3.6	Md	2.8	2.9
2000	8	19	17.92	-66.94	3	3.8	Md	3.4	3.4
2000	8	31	18.75	-64.00	74	4.1	Md	3.4	3.6
2000	9	3	18.70	-66.73	12	3.5	Md	2.7	2.7
2000	9	4	19.27	-65.99	107	3.5	Md	2.9	3.0
2000	9	4	19.05	-66.32	43	3.6	Md	3.4	3.4
2000	9	5	19.00	-68.09	113	4.1	Md	3.3	3.4
2000	9	7	18.87	-65.26	35	3.4	Md	2.8	2.8
2000	9	12	17.97	-65.93	5	3.6	Md	2.6	2.8
2000	9	15	18.87	-67.47	32	3.4	Md	3.2	3.2
2000	9	18	20.06	-70.07	33	4.4	mb	4.2	4.2
2000	9	24	19.47	-66.07	64	3.7	Md	3.0	3.1
2000	9	25	18.12	-67.29	18	3.1	Md	2.9	2.7
2000	9	27	19.11	-64.79	50	3.7	Md	2.8	3.0
2000	9	29	19.36	-66.27	27	3.7	Md	3.1	3.1
2000	9	30	19.42	-65.12	28	3.9	Md	3.4	3.5
2000	10	1	18.88	-64.66	25	3.5	Md	3.0	3.0
2000	10	2	18.90	-68.31	41	4.0	Md	3.5	3.5
2000	10	2	18.17	-67.41	7	3.7	Md	3.0	3.1
2000	10	8	18.78	-64.26	37	3.7	Md	3.1	3.2
2000	10	9	19.19	-65.40	90	3.9	Md	3.4	3.5
2000	10	11	18.93	-64.41	25	3.7	Md	3.0	3.1
2000	10	11	18.98	-66.60	68	3.1	Md	2.7	2.6
2000	10	13	18.64	-66.47	71	3.3	Md	2.8	2.8
2000	10	14	19.04	-67.42	30	3.2	Md	2.9	2.8
2000	10	15	18.55	-65.11	20	3.6	Md	2.9	2.9
2000	10	16	19.21	-64.48	45	4.0	Md	3.6	3.5
2000	10	17	18.81	-67.34	6	3.5	Md	2.8	2.9

2000	10	22	19.03	-64.96	68	3.8	Md	3.0	**3.1**
2000	10	23	18.79	-65.03	53	3.8	Md	3.0	**3.0**
2000	10	25	17.85	-66.91	41	3.8	Md	3.0	**3.1**
2000	10	25	17.86	-66.91	39	3.9	Md	3.3	**3.4**
2000	10	29	17.98	-66.94	16	3.6	Md	3.4	**3.4**
2000	10	30	18.71	-67.34	21	3.7	Md	3.4	**3.4**
2000	11	1	18.44	-67.05	102	3.4	Md	2.7	**2.8**
2000	11	6	18.00	-68.81	94	3.6	Md	3.2	**3.2**
2000	11	25	17.78	-65.97	46	3.2	Md	2.8	**2.9**
2000	11	30	18.63	-66.71	85	4.1	Md	3.6	**3.6**
2000	12	1	18.56	-66.68	86	3.1	Md	2.7	**2.7**
2000	12	1	19.30	-67.95	55	4.3	Md	4.0	**4.0**
2000	12	8	17.86	-68.55	35	3.7	Md	3.4	**3.4**
2000	12	9	18.82	-64.34	33	4.2	mb	3.7	**3.7**
2001	10	16	20.02	-69.17	33	4.5	mb	4.0	**4.1**
2001	10	17	19.35	-64.93	33	6.0	Mw	4.9	**5.9**
2001	10	17	18.37	-67.62	25	4.6	mb	4.4	**5.3**
2001	10	18	19.38	-64.84	33	4.5	mb	4.2	**4.3**
2001	10	22	19.31	-64.71	33	4.8	Md	4.6	**4.9**
2001	10	24	19.33	-65.02	48	5.1	mb	4.7	**5.1**
2001	11	27	17.90	-67.96	59	4.8	mb	4.4	**4.5**
2002	1	15	19.42	-64.18	33	4.8	mb	4.2	**4.9**
2002	4	11	19.30	-66.71	47	4.6	mb	4.3	**4.4**
2002	10	1	18.81	-63.06	41	4.9	mb	4.5	**4.9**
2002	10	18	19.50	-64.33	33	4.9	Md	4.1	**4.6**
2002	11	10	19.31	-63.64	33	4.8	Md	4.1	**4.6**
2002	12	21	18.36	-62.38	52	4.9	mb	4.5	**4.9**

Table 2. The reported CMT moment magnitude in catalogue (Mw) and the estimated **M** (this paper) for earthquakes in Puerto Rico.

Date	Distance (km)	Depth (km)	Mw(catalogue)	**M**(this study)
1996,05,11	186	35	5.1	5.2
1998,08,10	470	58	5.2	4.6
1999,01,18	144	33	5.0	4.8
2001,10,17	191	33	6.0	5.9

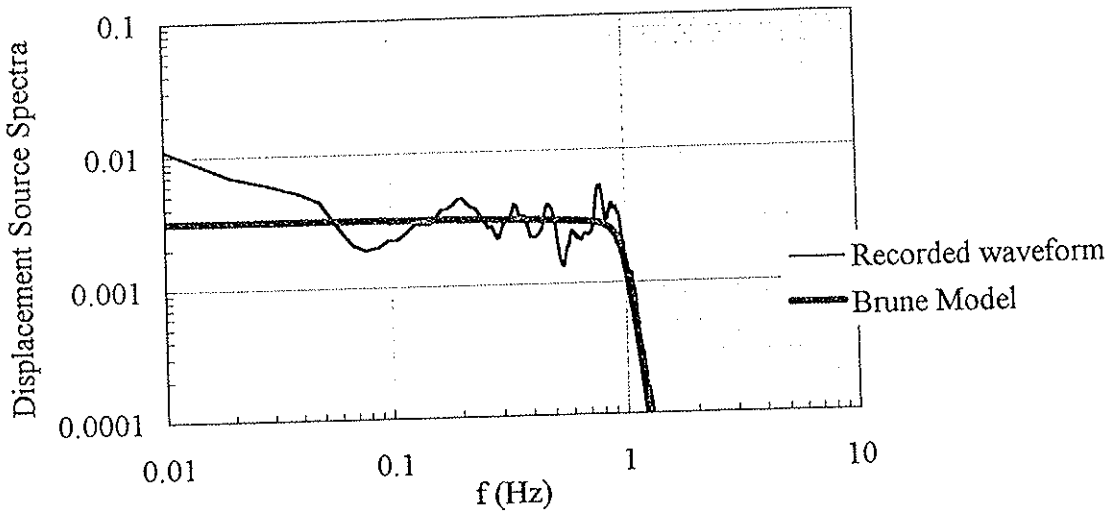

Figure 1.The displacement source spectrum of a M4.8 earthquake and the Brune source displacement spectrum model for that earthquake. The flat portion of the spectrum lies between 0.1 and 0.8 Hz (approximately).

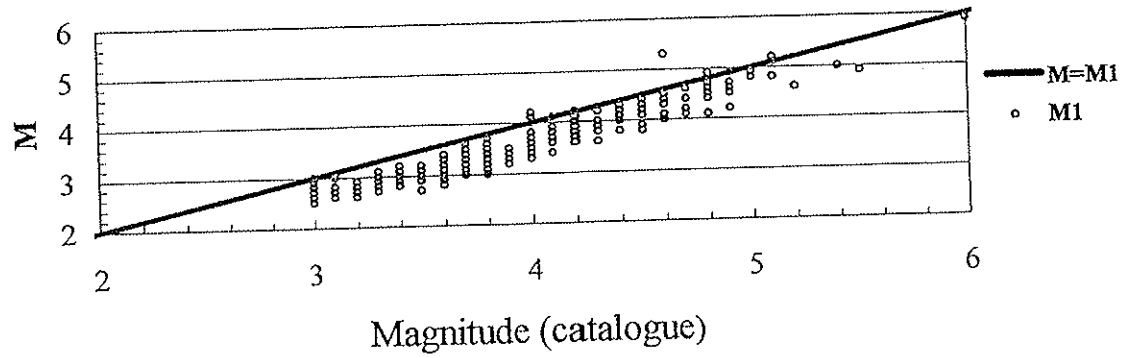

Figure 2. **M** versus catalogue magnitude based on the recorded waveforms at IRIS broadband station (SJG) in Puerto Rico. The catalogue magnitude is MD for all earthquakes of of M<4, and mb for all M>4.

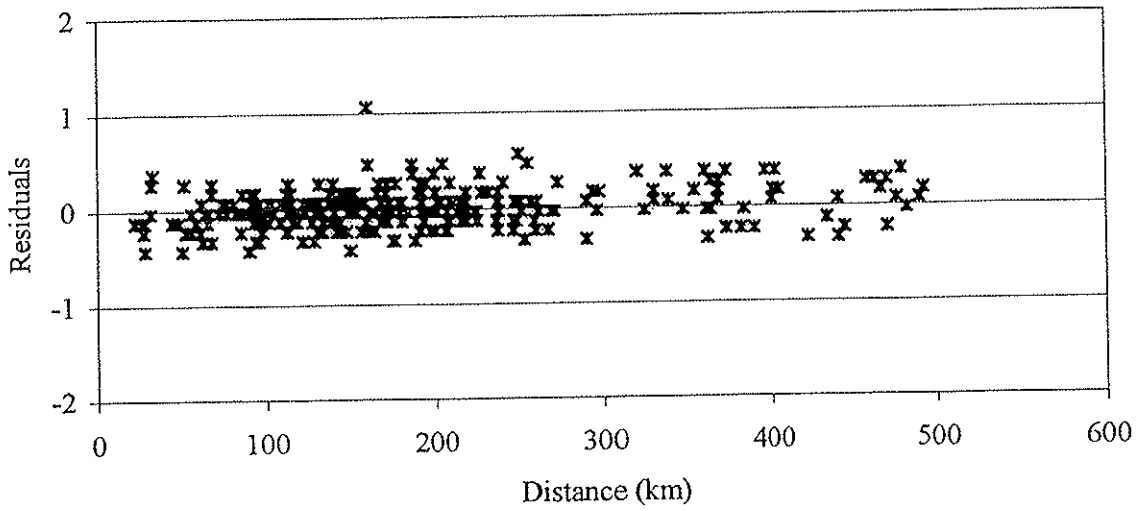

Figure 3. Residuals (**M**–Mcat+0.4) versus distance. There are no obvious distance-dependent trends in the obtained residuals, indicating the attenuation corrections are working well.

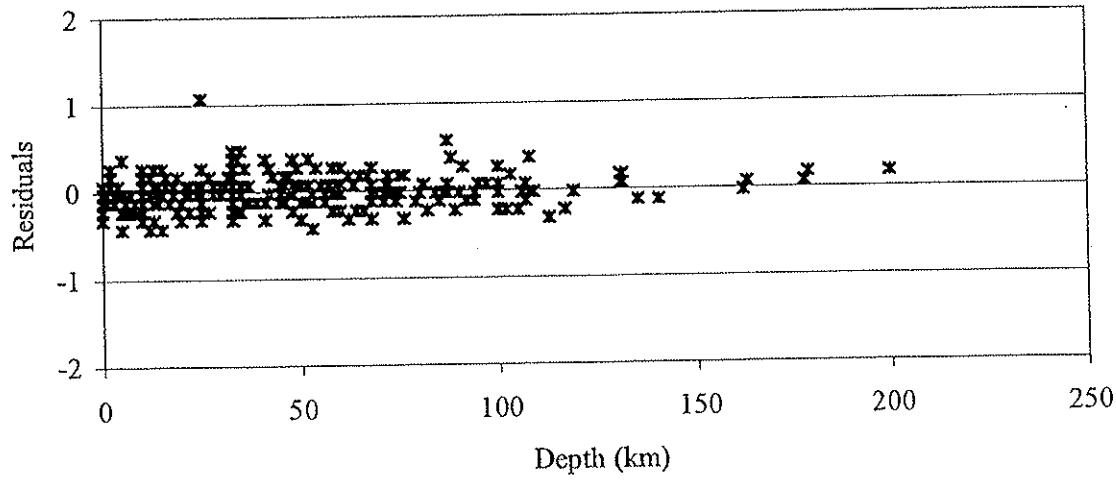

Figure 4. Residuals (M–Mcat+0.4) versus depth. There are no obvious depth-dependent trends in the obtained residuals, indicating the attenuation corrections are working well.

Figure 5. Profiles of observation points for an earthquake fault.

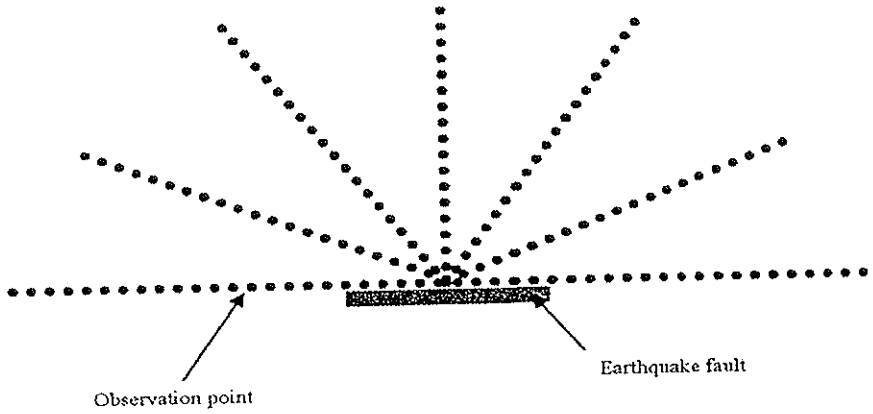

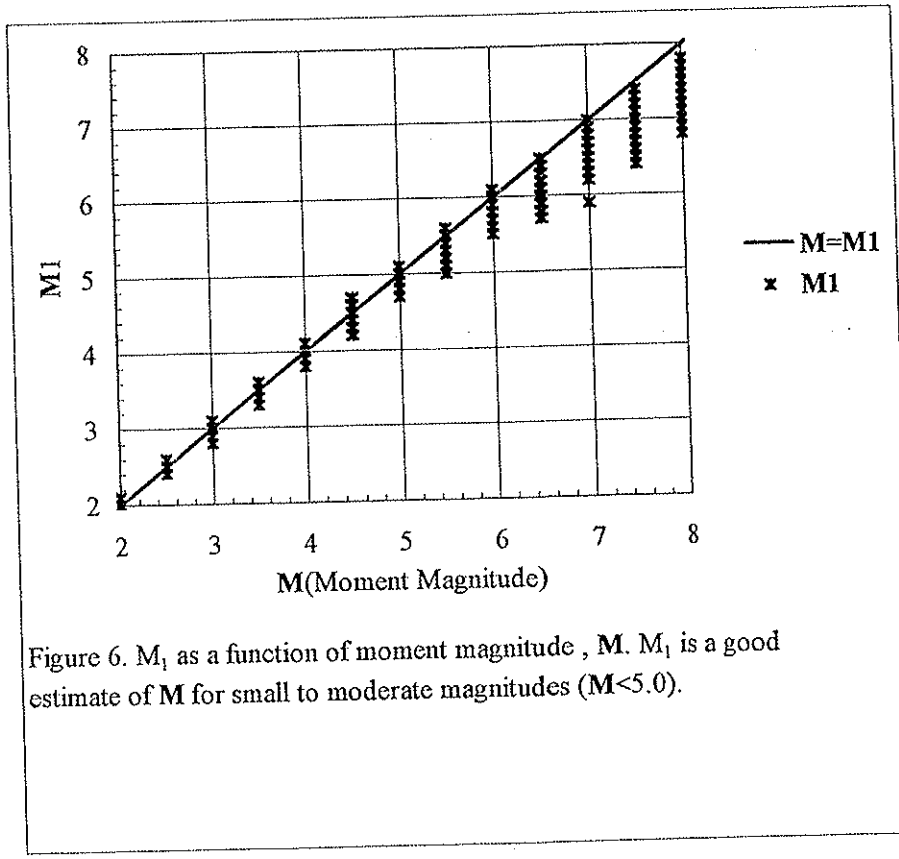

Figure 6. M_1 as a function of moment magnitude , **M**. M_1 is a good estimate of **M** for small to moderate magnitudes (**M**<5.0).

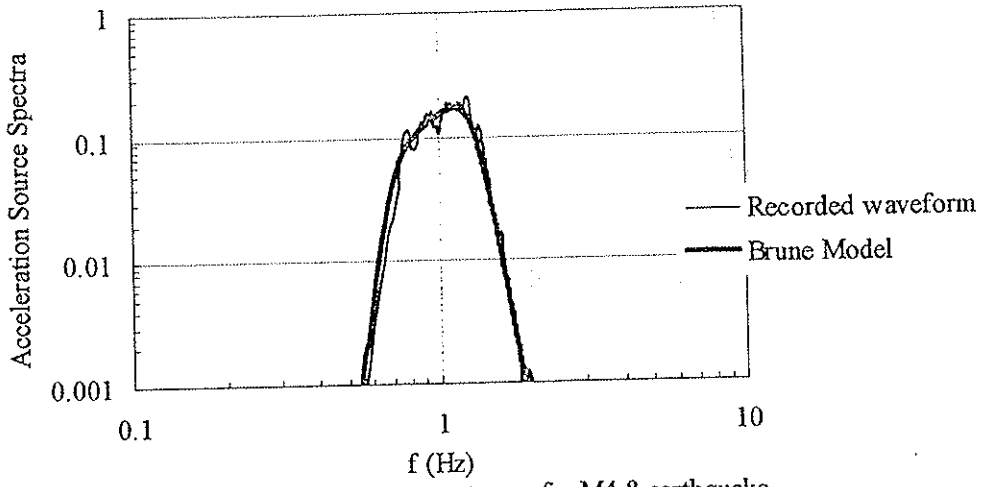

Figure 7.The acceleration source spectrum of a M4.8 earthquake and the corresponding Brune source spectrum model for that earthquake, after application of the Butterworth filters around 1 Hz.

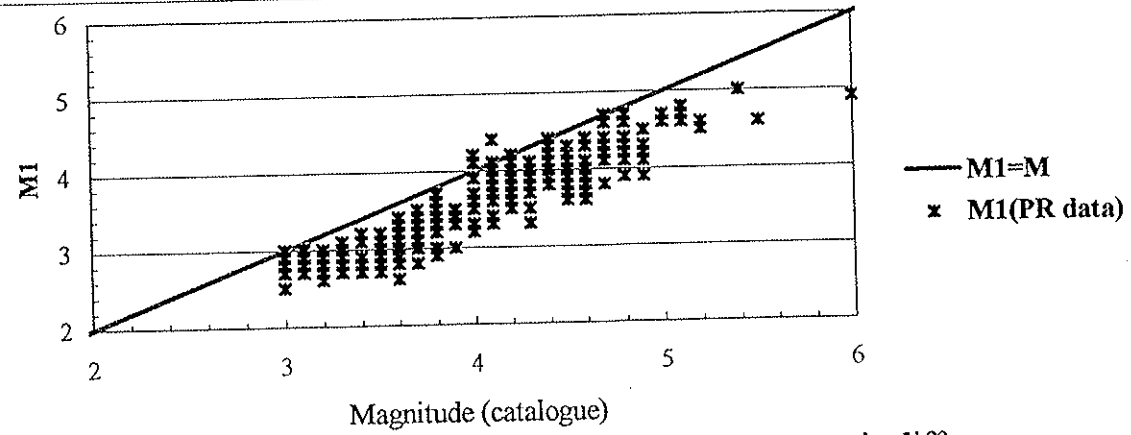

Figure 8. M_1 versus catalogue magnitude. There is a systematic difference between M_1 and catalogue magnitude, with the average difference of 0.4 units.

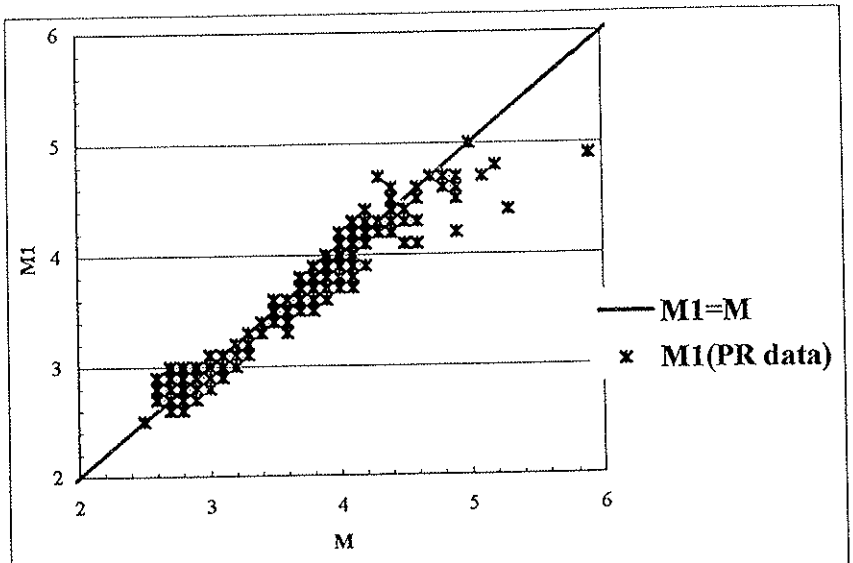

Figure 9. M_1, which is based on the amplitude of acceleration source spectra at 1 Hz, versus **M**, which is moment magnitude based on the displacement spectra at lower frequencies. M1 is a good estimate of **M** for earthquakes with magnitude less than M5.0.

Appendix A: EXSIM, a stochastic finite fault modeling program introducing the concept of dynamic corner frequency

The stochastic model is a commonly used tool for ground motion simulation. The method models ground motion as band limited Gaussian noise, whose amplitude spectrum is given by a seismological model (Boore, 1983). The most commonly-used seismological model for stochastic simulations has been the Brune (1970, 1971) point source model (e.g. Toro et al., 1997), However, point source models are inappropriate for large earthquakes. The effects of a large finite source, including fault geometry, heterogeneity of slip on the fault plane and directivity, can profoundly influence the amplitudes, frequency content and duration of ground motion. Finite-fault effects in ground motions become important for earthquakes with magnitudes exceeding approximately 6.0.

Finite fault modeling has been an important tool for the prediction of ground motion near the epicenters of large earthquakes (Hartzel, 1978; Irikura, 1983; Joyner and Boore, 1986; Heaton and Hartzel, 1986; Somerville et al., 1991; Tumarkin and Archuleta, 1994; Zeng et al., 1994; Beresnev and Atkinson, 1998a). One of the most useful methods to simulate ground motion for a large earthquake is based on the simulation of a number of small earthquakes as subfaults that comprise a big fault. A large fault is divided into N subfaults and each subfault is considered as a small point source (introduced by Hartzel, 1978). The rupture spreads radially from the hypocenter. In our implementation, the ground motions of subfaults, each of which are calculated by the stochastic point-source method, are summed with a proper delay time in the time domain to obtain the ground motion from the entire fault, a(t):

$$a(t)=\sum_{i=1}^{nl}\sum_{j=1}^{nw} a_{ij}(t+\Delta t_{ij}) \qquad (1)$$

where *nl* and *nw* are the number of subfaults along the length and width of main fault, respectively ($nl*nw = N$), Δt_{ij} is the relative delay time for the radiated wave from the ij^{th} subfault to reach the observation point. The $a_{ij}(t)$ are each calculated by the stochastic point source method. The acceleration spectrum for a subfault at a distance R_{ij} is modeled as a point source with an ω^2 shape (Aki, 1967; Brune, 1970; Boore 1983). The acceleration spectrum of shear wave of the ij^{th} subfault, $A_{ij}(f)$, is:

$$A_{ij}(f)=CM_{0ij}(2\pi f)^2/[1+(f/f_{0ij})^2]\exp(-\pi f\kappa)\exp(-\pi f R/Q\beta)/R_{ij}S_{ij}(f) \qquad (2)$$

where M_{0ij}, f_{0ij} and R_{ij} are the ij^{th} subfault seismic moment, corner frequency and distance from the observation point, respectively. Corner frequency, f_{0ij}, is given by $f_{0ij}=4.9e+6\,\beta\,(\Delta\sigma / M_{0ij})^{1/3}$ where $\Delta\sigma$ is stress drop in bars M_{0ij} is in dyne-cm and β is shear wave velocity in km/s. The constant $C=\Re^{\theta\varphi}\,F\,V/(4\pi\rho\beta^3)$, where $\Re^{\theta\varphi}$ = radiation pattern (average value of 0.55 for shear waves), F= free surface amplification (2.0), V= partition onto two horizontal components (0.71), ρ= density and β is shear wave velocity (Boore, 1983). $\exp(-\pi f\kappa)$ is a high cut filter to model near-surface "*kappa*" effects: this is the commonly-observed rapid spectral decay at high

frequencies. The quality factor, Q, is inversely related to anelastic attenuation. $S(f)$ represents site amplification (=1 for a very hard rock site).

The moment of each subfault is controlled by the ratio of its area to the area of the main fault ($M_{oij}=M_o/N$ where M_0 is the seismic moment of the entire fault). If the subfaults are not identical we can express the seismic moment of each subfault as:

$$M_{oij} =(M_o S_{ij})/(\sum_{l=1}^{nl} \sum_{k=1}^{nw} S_{kl}) \quad (3)$$

where S_{ij} is the relative slip weight of the ijth subfault. Earthquake time history simulation deals with the time from the beginning of rupture to the time when the rupture stops. In our finite fault model we deal with a ruptured area that is time dependent; it is initially zero and is finally equal to the entire fault area. Corner frequency is inversely proportional to the ruptured area. Therefore in time history simulation the corner frequency may be considered as a function of time. The rupture begins with high corner frequencies and progresses to lower corner frequencies. We suppose that, during an earthquake, at each moment of time the corner frequency is dependent on the cumulative ruptured area. The rupture history controls the frequency content of the simulated time series.

In our dynamic approach, the corner frequency of the first subfault (near the beginning of rupture) is $f_{011}=S\ 4.9e+6\ \beta\ (\Delta\sigma / M_{011})^{1/3}$, where M_{011} is the seismic moment of the first subfault. The dynamic corner frequency of the ijth subfault, $f_{oij}(t)$, can be defined as a function of $N_R(t)$, the cumulative number of ruptured subfaults at time t.

$$f_{oij}(t)= N_R(t)^{-1/3} S\ 4.9e+6\ \beta\ (\Delta\sigma / M_{oave})^{1/3} \quad (4)$$

where $M_{oave} = M_o/ N$ is the average seismic moment of subfaults and S is a constant. As the rupture proceeds towards the end of the fault the number of ruptured subfaults increases and, based on equation 4, the corner frequency of the subfaults decreases. The dynamic corner frequency concept will tend to decrease the level of the spectrum and the radiated energy ($A_{ij}(f)_{f>>fijo} \propto f_{oij}^2$) of subfaults as the rupture progresses. We need to introduce a scaling factor to conserve the total radiated energy. The total radiated energy from each subfault should be the same since all of the subfaults are identical in this step. The acceleration spectrum of the ijth subfault, $A_{ij}(f)$, is thus:

$$A_{ij}(f)=C\ M_{oij}\ H f^2 /[1+(f/f_{oij})^2] \quad (5)$$

$$H = (N\int \{f^2/ [1+(f/ f_0)^2]\}^2\ df / \int \{ f^2/ [1+(f/f_{oij})^2]\}^2\ df)^{1/2} \quad (6)$$

where H is a scaling factor to conserve the total radiated energy. Thus, the diminishing effect of f_{oij} on the total radiated energy from the subfault is compensated for by the scaling factor, in order to keep the total radiated energy unchanged. The total radiated energy from the ijth subfault is equal to the total radiated energy from the first subfault, but the calculation of corner frequency, which controls the shape of the spectrum, comes from the total ruptured area. In other words, the total radiated energy remains unchanged but the distribution of energy tends to shift towards lower frequencies.

The new simulation approach is implemented in a modified version of the computer program FINSIM (Beresnev and Atkinson, 1998b). FINSIM is a well-known stochastic finite-fault

simulation program that has been validated using data from many real earthquake faults, including Michoacan, Mexico (1985); Lama Prieta (1989); Northridge (1994); Valparaiso, Chile (1985); and Saguenay, Quebec (1988) (Beresnev and Atkinson 1997, 1998a, 1998b, 1999, 2000, 2001).The modified program has been renamed EXSIM. The modifications include the following features.

- Inclusion of the new concept of "dynamic corner frequency"
- Elimination of multiple triggering of subfaults.
- Variability of pulsing area, or the number of subfaults which are considered as active subfaults in the calculation of dynamic corner frequency (this allows for self-healing slip models).
- Calculation of subfault seismic moment based on dividing the total seismic moment of the earthquake fault by the number of subfaults

In the new approach, the total radiated energy from the fault and the total seismic moment are conserved independent of subfault size over a wide range of subfault sizes. The total radiated energy from a subfault is calculated based on the size of subfault and a weighting function, but the calculation of corner frequency, which controls the shape of spectrum, comes from the total ruptured area. The moment of each subfault is controlled by the ratio of its area to the area of the main fault ($M_{0i}=M_0/N$). If the subfaults are not identical we apply a weighting function for each subfault based on the relative slips of subfaults.

Limiting the number of active subfaults in the calculation of dynamic corner frequency can simulate the notion of self-healing slip pulses. EXSIM allows for variability in the "pulsing area" or the number of subfaults, which are considered as active subfaults, in the calculation of dynamic corner frequency. In EXSIM the percentage of pulsing area on the fault will affect the relative amplitudes of low-frequency motion in finite fault modeling. Variation of stress parameter can be used to adjust the relative amplitudes of high-frequency motion. By increasing stress parameter, the amplitude of high frequencies increases.

A generic EXSIM model was derived which matches (in terms of predicted ground motions) the generic FINSIM model results for North America (Beresnev and Atkinson, 2001). The rationale for this calibration is that FINSIM has been extensively validated against real earthquake data over a wide range of conditions. The calibrated EXSIM model produces approximately the same peak ground motions and response spectra as the FINSIM model of Beresnev and Atkinson (1998b), and provides good characterization of the main seismological effects, including source and path, for extended fault sources. The advantage of EXSIM is that it introduces conceptual improvements, such as independence of results from subfault size and conservation of radiated energy, and allows simulation of self-healing slip pulses.

References

Aki, K. (1967). Scaling law of seismic spectrum, J. Geophys. Res. 72, 1217-1231.

Beresnev, I. and G. Atkinson (1998a). Stochastic finite-fault modeling of ground motions from the 1994 Northridge, California earthquake. I. Validation on rock sites. Bull. Seism. Soc. Am., **88**, 1392-1401.

Beresnev, I. and G. Atkinson (1997). Modeling finite fault radiation from the w^n spectrum. Bull. Seism. Soc. Am., **87**, 67-84.

Beresnev, I. and G. Atkinson (1998a). Stochastic finite-fault modeling of ground motions from the 1994 Northridge, California earthquake. I. Validation on rock sites. Bull. Seism. Soc. Am., **88**, 1392-1401.

Beresnev, I. and G. Atkinson (1998b). FINSIM - a FORTRAN program for simulating stochastic acceleration time histories from finite faults. Seism. Res. L., **69**, 27-32.

Beresnev, I. and G. Atkinson (1999). Generic finite-fault model for ground motion prediction in eastern North America. Bull. Seism. Soc. Am., **89**, 608-625.

Beresnev, I. and G. Atkinson (2000). Subevent structure of large earthquakes – a ground motion perspective. Geophys. Res. L.,**28**, 53-56.

Beresnev, I. and G. Atkinson (2001). Source parameters of earthquakes in eastern and western North America based on finite-fault modeling. Bull. Seism. Soc. Am., **91**, submitted.

Beresnev, I., G. Atkinson, P. Johnson and E. Field (1998). Stochastic finite-fault modeling of ground motions from the 1994 Northridge, California earthquake. II. Widespread nonlinear response at soil sites. Bull Seism. Soc. Am., **88**, 1402-1410.

Boore, D. (1983). Stochastic simulation of high-frequency ground motions based on seismological models of the radiated spectra. Bull. Seism. Soc. Am., **73**, 1865-1894.

Brune, J. (1970). Tectonic stress and the spectra of seismic shear waves from earthquakes. J. Geophys. Res., **75**, 4997-5009.

Brune, J. (1971). Correction. J. Geophys. Res., 76, 5002.

Hartzell, S. (1978). Earthquake aftershocks as Green's functions. Geophys. Res. Letters, **5**, 1-14.

Heaton, T., and S. Hartzell (1986). Source characteristics of hypothetical subduction earthquakes in the Northwestern United States. Bull. Seism. Soc. Am., **76**, 675-708.

Irikura, K. (1983). Semi-empirical estimation of strong ground motions during large earthquakes. Bull. Disaster Prevention Res. Inst., Kyoto Univ., **33**, 63-104.

Joyner, W. and D. Boore (1986). On simulating large earthquakes by Green's function additon of smaller earthquakes. In: Earthquake Source Mechanics. Maurice Ewing Volume 6. Geophys. Monogr. Am. Geophys. Union, **37**, 269-274.

Somerville, P., M. Sen and B. Cohee (1991). Simulations of strong ground motions recorded during the 1985 Michoacan, Mexico and Valparaiso, Chile, earthquakes. Bull. Seism. Soc. Am., **81**, 1-27.

Tumarkin, A. and R. Archuleta (1994). Empirical ground motion prediction. Annali Di Geofisica. 37, 1691-1720.

Zeng, Y., J. Anderson and G. Yu (1994). A composite source model for computing realistic synthetic strong ground motions. Geophys. Res. L.